Extended Source Analysis Issues

1 Introduction

Analyzing the **ACIS** CCD spectrum for a *Chandra* observation of a point source is in principle a relatively straight-forward process. The detected events from a relatively small region around the source position are extracted and binned to produce a PHA spectrum file. This file is then used in conjunction with a CCD response matrix (RMF file) and effective area file (ARF file) calculated for the relevant source position on the CCD. Given this triplet of files, one can use programs such as *Sherpa* or *XSPEC* to compare various model spectra against the observed CCD spectrum. For extended sources, this paradigm becomes more complicated because the response function of the **ACIS** CCDs varies as a function of position on the chip. In the following discussion, we will describe the current state of the **ACIS** response calibration and provide some guidelines for users analyzing spectral data from extended sources.

2 Definitions

To begin, let us define a few relevant terms. For more detailed information on these topics, the reader is referred to *The Chandra Proposers' Observatory Guide* and the *CIAO Instrument and Calibration Guide.*

PHA	Detector pulse height channel. Proportional to photon energy.
Gain	Conversion factor between photon energy and PHA.
PI	Pulse invariant detector channel. Basically a uniformly binned energy.
Response function	Function mapping the energy of a photon into detector PHA channel. This function depends on position on the CCD and energy.
PHA file	Histogram of counts per PHA channel.
PI file	Histogram of counts per PI channel.
RMF file	Discrete matrix resprentation of the response function.
FEF file	FITS file containing an analytic or tabulated function. Used by CIAO to create RMF files.
ARF file	Ancillary response file. File containing effective area versus energy.

3 Spectral Analysis

Traditionally, an extended source would be an object for which the intrinsic spatial distribution of the object is larger than the point spread function (PSF) of the telescope. For the purposes of this discussion, however, the relevant spatial scale is not the telescope PSF but rather the scale on which the response function of the detector changes appreciably. As we discuss in §4, the current **ACIS** calibration has determined the response function over regions 32x32 pixels, 64x64 pixels, and 256x32 pixels in size for the S3 BI, S5 BI, and FI chips, respectively. These regions are much larger than the **HRMA** PSF with the exception of point sources far off-axis.

3.1 Point Sources

We note that analysis of traditional point source objects is not completely immune to the effects of a spatially varying response function. The standard *Chandra* dither motion follows a lissajous pattern tracing out a region roughly 30x30 pixels. Although the aspect reconstruction removes these offsets when producing the Sky X and Y coordinates, the detected events will still exhibit gain and resolution variations if the dither pattern encompasses more than one response region. The variations associated with adjacent response regions are likely to be small (<5%) unless a CCD node boundary is crossed.

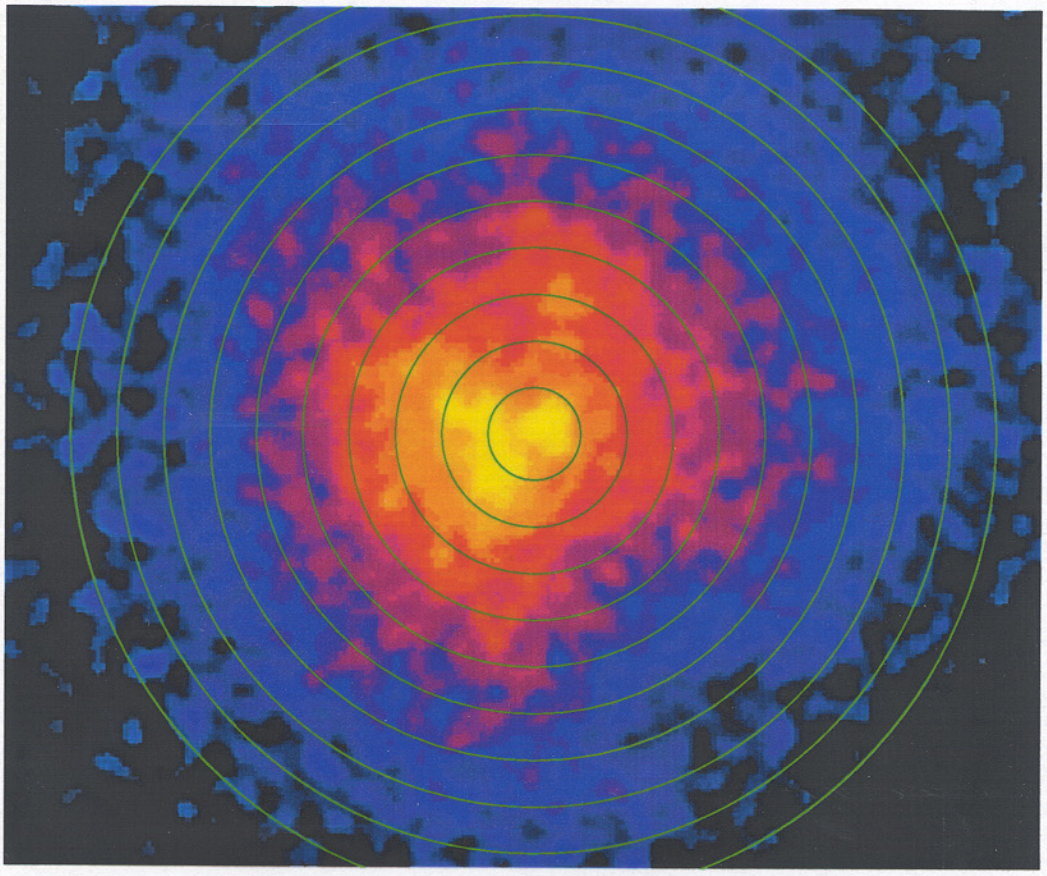

Figure 1: ACIS-S3 image of the Hydra A cluster of galaxies. A series of annular extraction regions are shown with fixed widths of 10 Sky pixels.

3.2 Extended Sources

Larger sources such as galaxies, clusters, and supernova remnants will typically illuminate multiple, different response regions regardless of the dither motion. For these objects, variations in the **ACIS** response within a given extraction region can be significant. Figure 1 shows a typical spectral analysis scenario for a cluster of galaxies. In this example, the cluster Hydra A is shown with a set of annular extraction regions 10 Sky pixels in width superimposed. This particular observation was imaged on the ACIS–S3 CCD which exhibits 1024, 32x32 pixel response regions. In Figure 2, the 40 or so independent response regions associated with one of the annuli are shown.

3.3 Averaging Response Matrices

Ideally, one would like to associate a single RMF and ARF file with the PHA or PI file extracted for each annular region. However, as Figure 2 illustrates, each of these annular extraction regions spans many response regions. To analyze the spectrum from one of the annular regions shown in Figure 1, one must account for the spatial variations of the following components over the region: a) source spectrum, b) effective area, c) CCD gain, and d) CCD resolution. Given certain assumptions, "average" RMF and ARF can be constructed which take into account these variations. These assumptions, their limitations and a technique for constructing such average response files is discussed in more detail in Section 5 below.

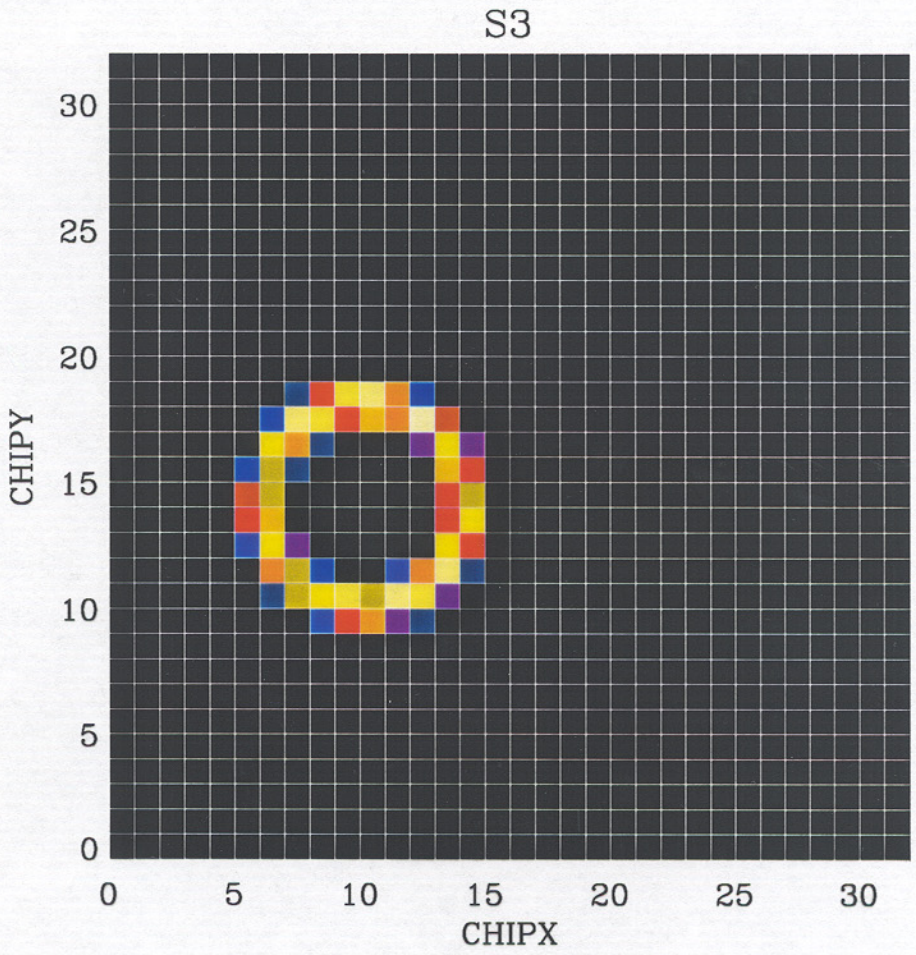

Figure 2: Image showing the various independent response regions encompassed by one of the annular extraction regions shown in Figure 1. The X and Y axes indicate the indices of the 1024 response regions which currently describe the response calibration of the S3 BI chip. The colorscale represents the number of counts detected in a given region.

4 The Current ACIS Calibration

The complexity of analyzing spectra such as those described above is primarily determined by the uniformity of the detector properties. For the purposes of this discussion, the relevant properties consist of the CCD gain, spectral resolution, and effective area each of which are discussed separately below. We concentrate primarily on the S3 and I3 aimpoint CCDs since they currently are the best calibrated. However, qualitatively the results for S3 and I3 can be extended to the other BI and FI chips. In addition, calibration data currently exists for two focal plane temperatures, -110 C and -120 C. These two different operating temperatures lead to differences in the spatial variation of detector properties. Where the data calibration allows, we present results for both temperatures.

4.1 Spatial Variations in Gain

The gain of a CCD describes the mapping between the incoming photon energy and the detected event pulse height amplitude (PHA) value. For the most part, CCDs are linear devices and the detected PHA value is directly proportional to the photon's energy. As currently calibrated, the gain for a given CCD is then simply the slope of this linear relationship [1]. For each of the 10 CCDs in the ACIS array, the CXC Calibration group has determined the gain as a function of position on the chip. Due to signal to noise considerations, the gain on the S3 chip has been determined in 32x32 pixel cells while the S1 chip was mapped in 64x64 pixels cells. For the FI chips, the parallel CTI dominates the gain variation resulting in a gradient in the gain which is virtually independent of CHIPX position for a given node. Consequently, the gain for each FI CCD has been determined in 256x32 pixel cells. These calibrations result in 1024, 256, and 128 independent gain measurements for the S3, S1, and FI chips, respectively.

The spatial non-uniformity of the ACIS gain is demonstrated in Figures 3–5.

4.2 Spatial Variations in Spectral Resolution

4.3 Spatial Variations in Effective Area

5 Averaging Response Matrices

5.1 Theory

Formally, we can write an expression for the total number of detected events, C, from a given spatial extraction region, Ω as

$$C(h) = \int_{\Delta E} dE \int_{\Omega} d\Omega \; A(\vec{r}, E) \; R(\vec{r}, E, p) \; S(\vec{r}, E) \tag{1}$$

where h represents a pulse height band, E is photon energy, R represents the detector redistribution function, and A is the effective area of the telescope. Here, S specifies the intrinsic spectral and spatial properties of the source. If Ω consists of multiple, smaller spatial regions, Ω_i, where the detector redistribution and effective area are assumed to be uniform, i.e.

$$R_i(\vec{r}, E, p) \approx R_i(\Delta E, p) \qquad A_i(\vec{r}, \Delta E) \approx A_i(\Delta E) \quad , \tag{2}$$

one may write

$$C(\Delta h) = \sum_{i=1}^{n} R_i(\Delta E, p) \; A_i(\Delta E) \int_{\Omega_i} S(\vec{r}, \Delta E) \; d\Omega_i \tag{3}$$

where we have also assumed a small range in energy, ΔE, such that the relevant terms do not vary greatly. Consequently, all of the following expressions are implicitly functions of energy. These regions of constant

[1] Strictly speaking, the PHA to photon energy mapping is non-linear. Deviations from a simple linear fit increase as one moves to lower photon energies. For both BI and FI chips, the magnitude of these deviations is roughly 5% down to 0.5 keV. An updated set of calibration data and `CIAO` software tools are currently being produced which take into account the non-linearity of the CCD gain.

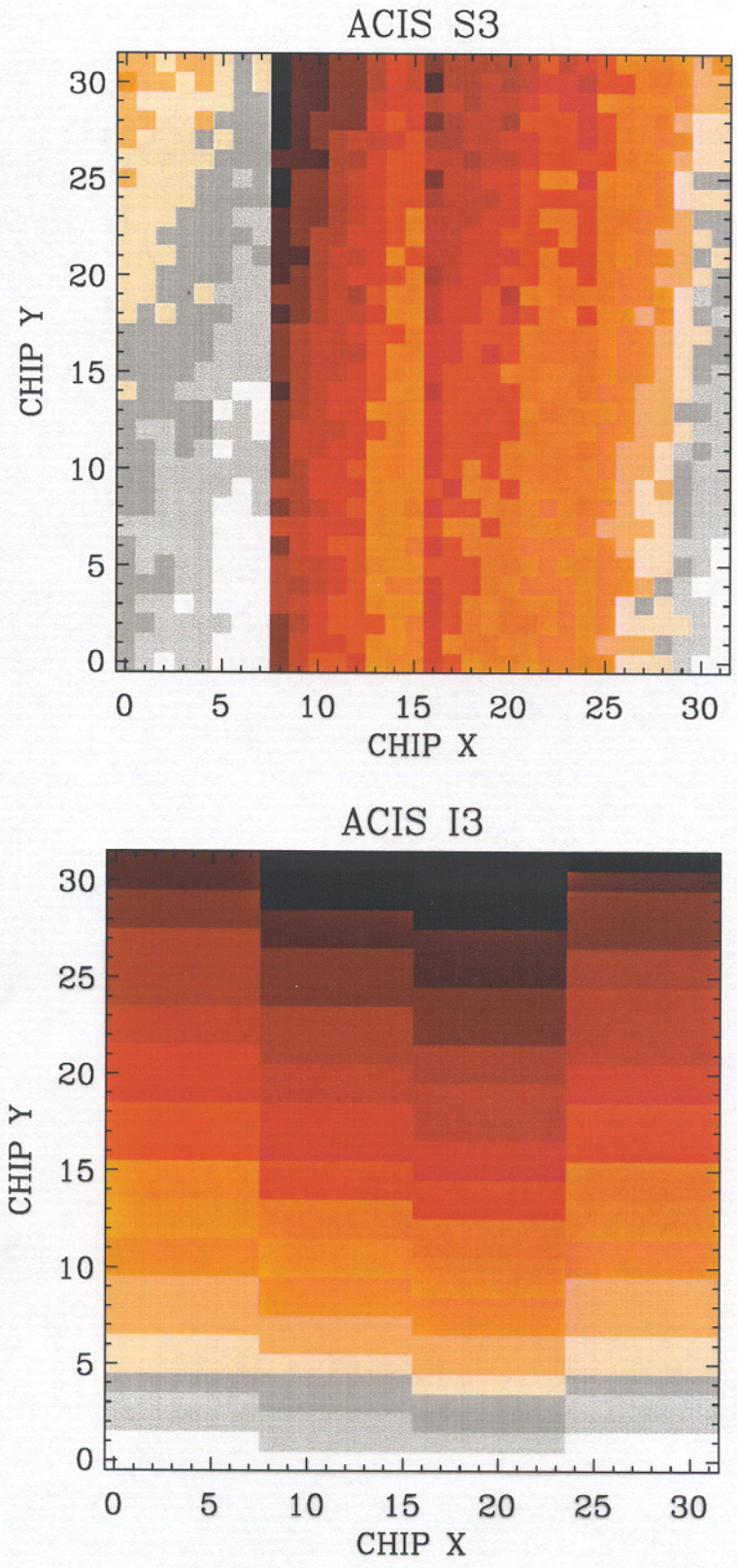

Figure 3: ACIS Gain variations. Notice the size of the squares.

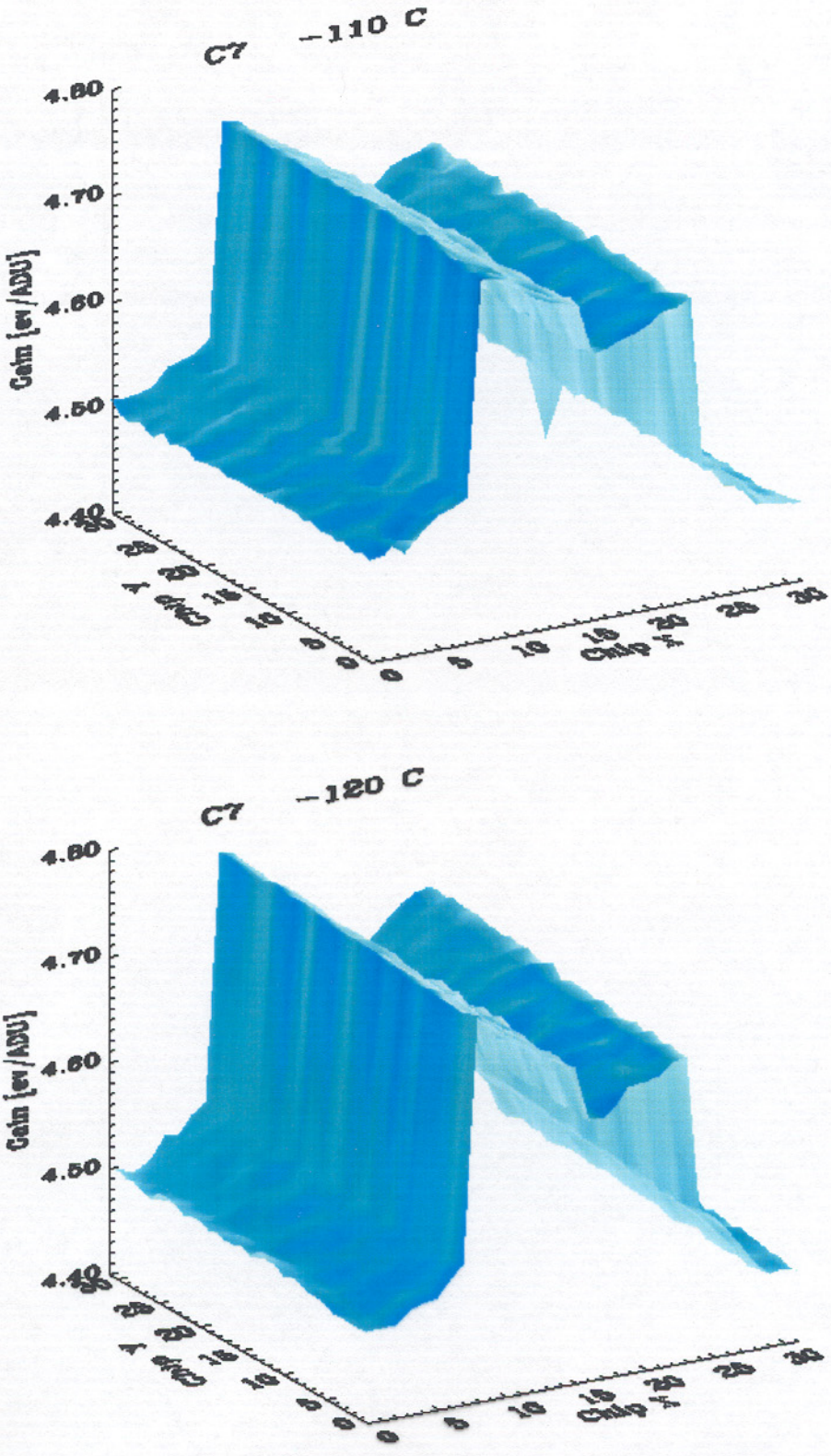

Figure 4: ACIS Gain variations. Notice the size of the squares.

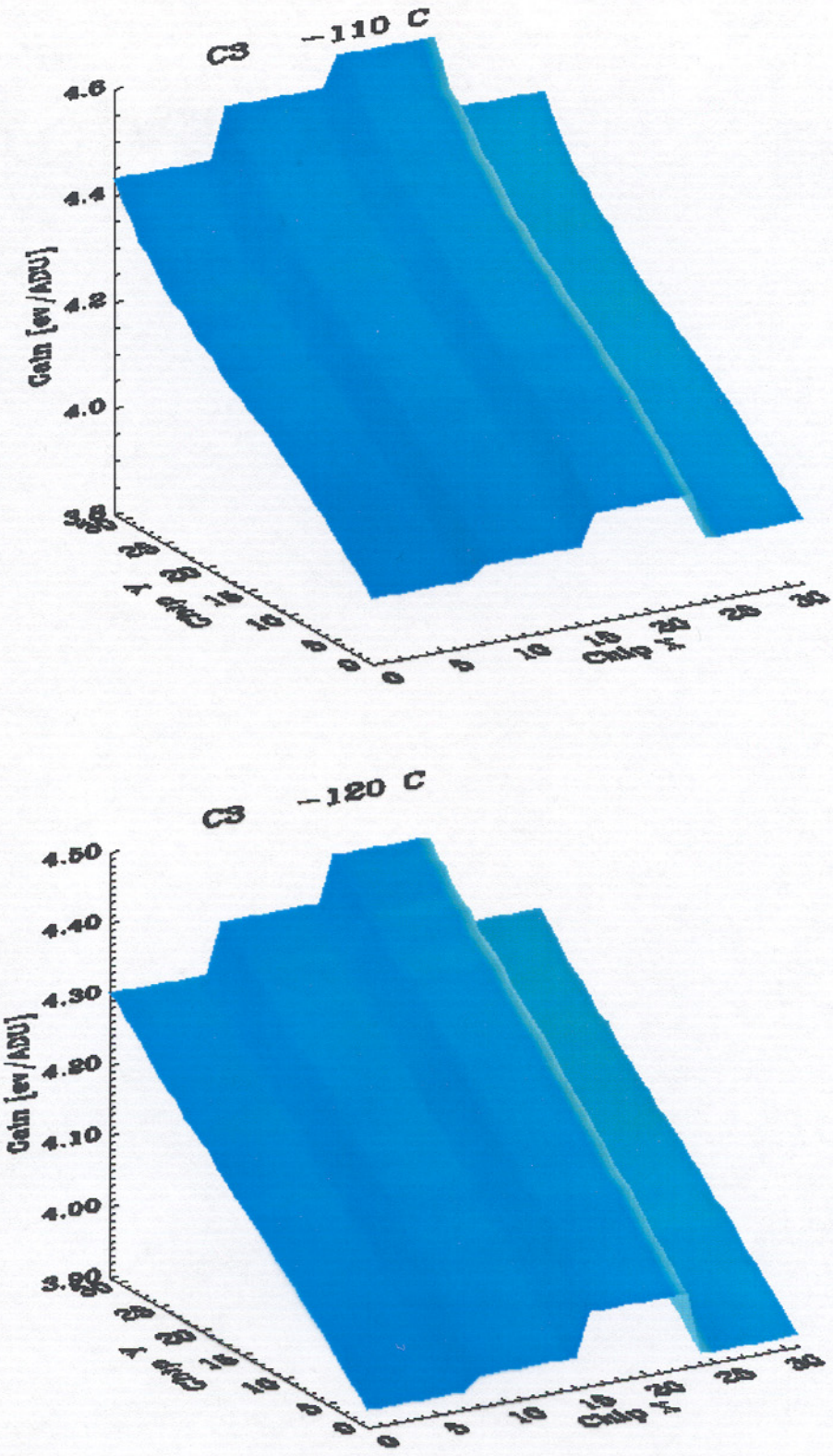

Figure 5: ACIS Gain variations. Notice the size of the squares.

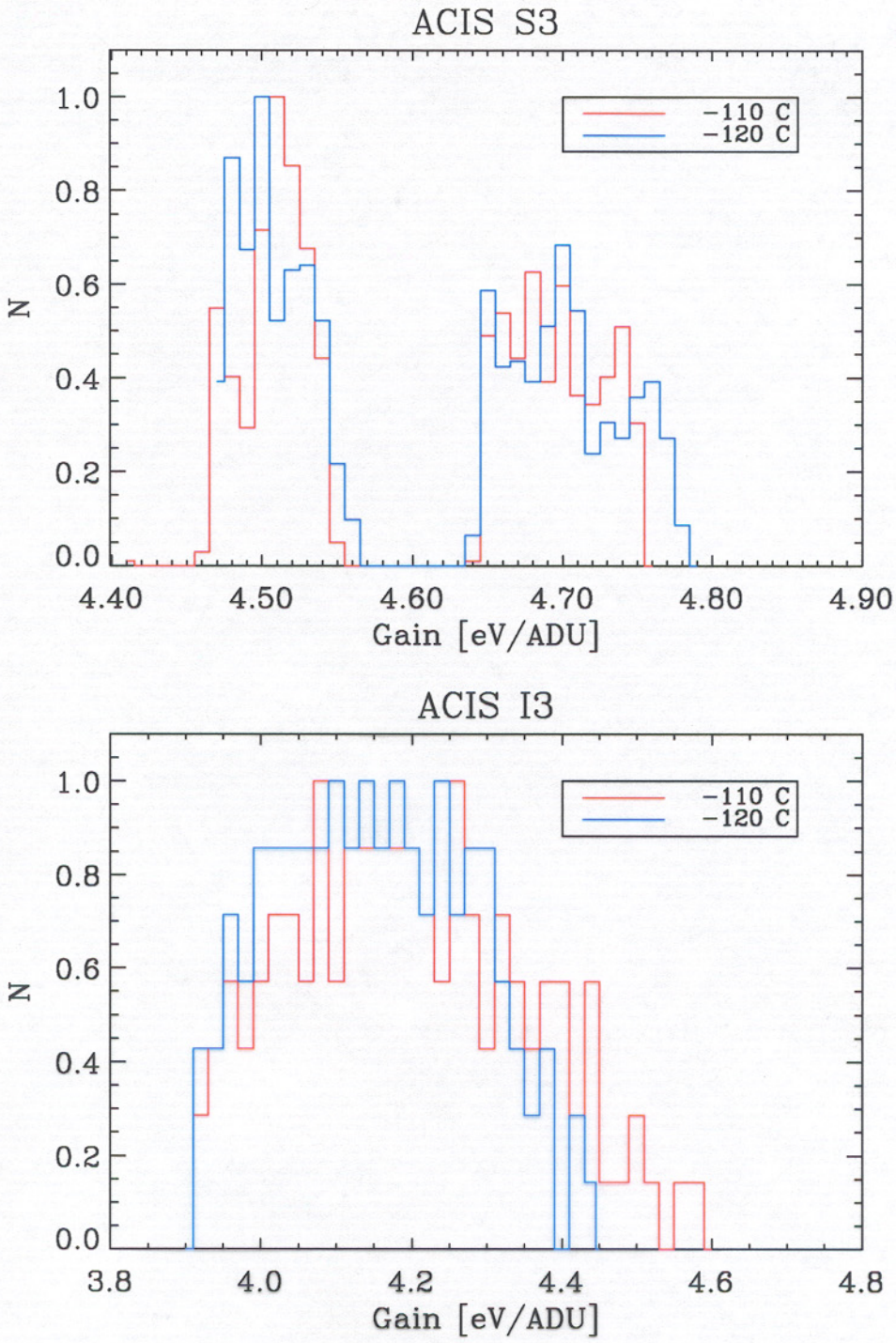

Figure 6: Histogram of ACIS S3 and I3 Gain Variations.

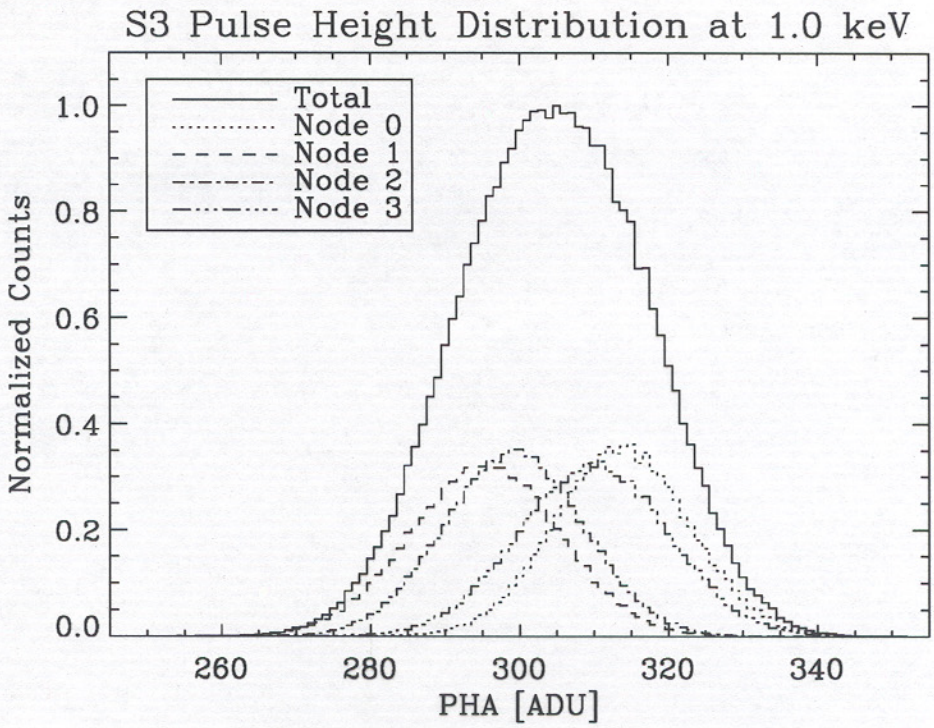

Figure 7: S3 Pulse Height Distribution at 1.0 keV.

$R(\Delta E, p)$ naturally correspond to the independent response regions determined by the ACIS calibration and discussed below in §4. The validity of the assumption $A_i(\vec{r}, \Delta E) \approx A_i(\Delta E)$ will depend on the size of the response regions and hence the type of CCD.

Evaluating equation 3 requires a model of the spectral and spatial variations of the source. For objects such as clusters, these models could be quite complicated given the possible presence of multiple temperature components, projection effects, spatially varying absorption, etc. Unfortunately neither *Sherpa* or *XSPEC* allow for fitting of spatially varying spectra. These programs assume the spectrum of the source is uniform over the extraction region being considered. In order to cast equation 3 in a form similar to that solved by *Sherpa* and *XSPEC*, we can define

$$S(\vec{r}, \Delta E) \approx S(\Delta E)\ \rho(\vec{r}, \Delta E) \tag{4}$$

$$w_i(\Delta E) = \int_{\Omega_i} d\Omega_i\ \rho(\vec{r}, \Delta E) \qquad \sum_{i=1}^{n} w_i(\Delta E) = \int_{\Omega} d\Omega\ \rho(\vec{r}, \Delta E) = 1 \quad . \tag{5}$$

Substituting these definitions into equation 3 yields

$$C(\Delta h) = S(\Delta E) \sum_{i=1}^{n} R_i(\Delta E, p)\ A_i(\Delta E)\ w_i(\Delta E) \tag{6}$$

where the weights, $w_i(\Delta E)$ contain the spatial variation of the source over the energy band ΔE. This equation is very similar to the equation which *Sherpa* and *XSPEC* solve when performing simultaneous fitting of multiple datasets. If we make the further definitions,

$$\bar{A}(\Delta E) = \frac{1}{n} \sum_{i=1}^{n} A_i(\Delta E)\ w_i(\Delta E) \qquad \bar{R}(\Delta E, p) = \sum_{i=1}^{n} R_i(\Delta E, p)\ a_i(\Delta E) \tag{7}$$

$$a_i(\Delta E) = \frac{A_i(\Delta E) w_i(\Delta E)}{n \bar{A}(\Delta E)} \tag{8}$$

then equation 6 can be written in the familiar form

$$C(\Delta h) = \bar{A}(\Delta E)\ \bar{R}(\Delta E, p)\ S(\Delta E) \tag{9}$$

where a single RMF and ARF file are associated with the selected extraction region. We note that the presence of dither will complicate the calculation of the various quantities since, although the extraction region is defined in Sky coordinates, the various response regions which define Ω_i are functions of detector coordinates. Further, the above expressions are also valid for point sources which span multiple response regions. In this case, $\rho(\vec{r}, \Delta E)$, is simply the **HRMA** PSF.

5.2 Caveats

Although familiar, equations 6 and 9 still require a model for the spatial variation of the source spectrum in order to calculate the weighting factors $w_i(\Delta E)$ and $a_i(\Delta E)$. Since this spatial model is not known *a priori*, it should be fit iteratively along with the intrinsic parameters of the spectral model. Neither *Sherpa* nor *XSPEC* currently support this type of model. In addition, the construction of $\bar{A}(\Delta E)$ and $\bar{R}(\Delta E, p)$ for each annulus in Figure 1 can quickly become computationally expensive, requiring the calculation of ~50-100 w_i and a_i per annulus per energy bin. For example, considering the Hydra A cluster analysis shown in Figure 1, we might have 50 response regions per annulus and 1000 energy points resulting in 5×10^4 weight calculations per annulus. Each of these weights should in principle be recomputed for each iteration in the fitting process.

In practice, the complexity involved in spectral analysis of extended sources can be reduced depending on the specifics of the particular source, quality of the data, and scientific goals.

- Source spectrum and spatial distribution are uncorrelated
- RMF does not vary over a given component region
- Effective area is uniform over a given component region
- The energy band in question is sufficiently narrow that all quantities are uniform over the energy band.

5.3 Accuracy

6 Guidelines

6.1 PI or PHA space?

PI.

6.2 One RMF or Many?

BI chip — One. FI chip — Many.

7 Summary

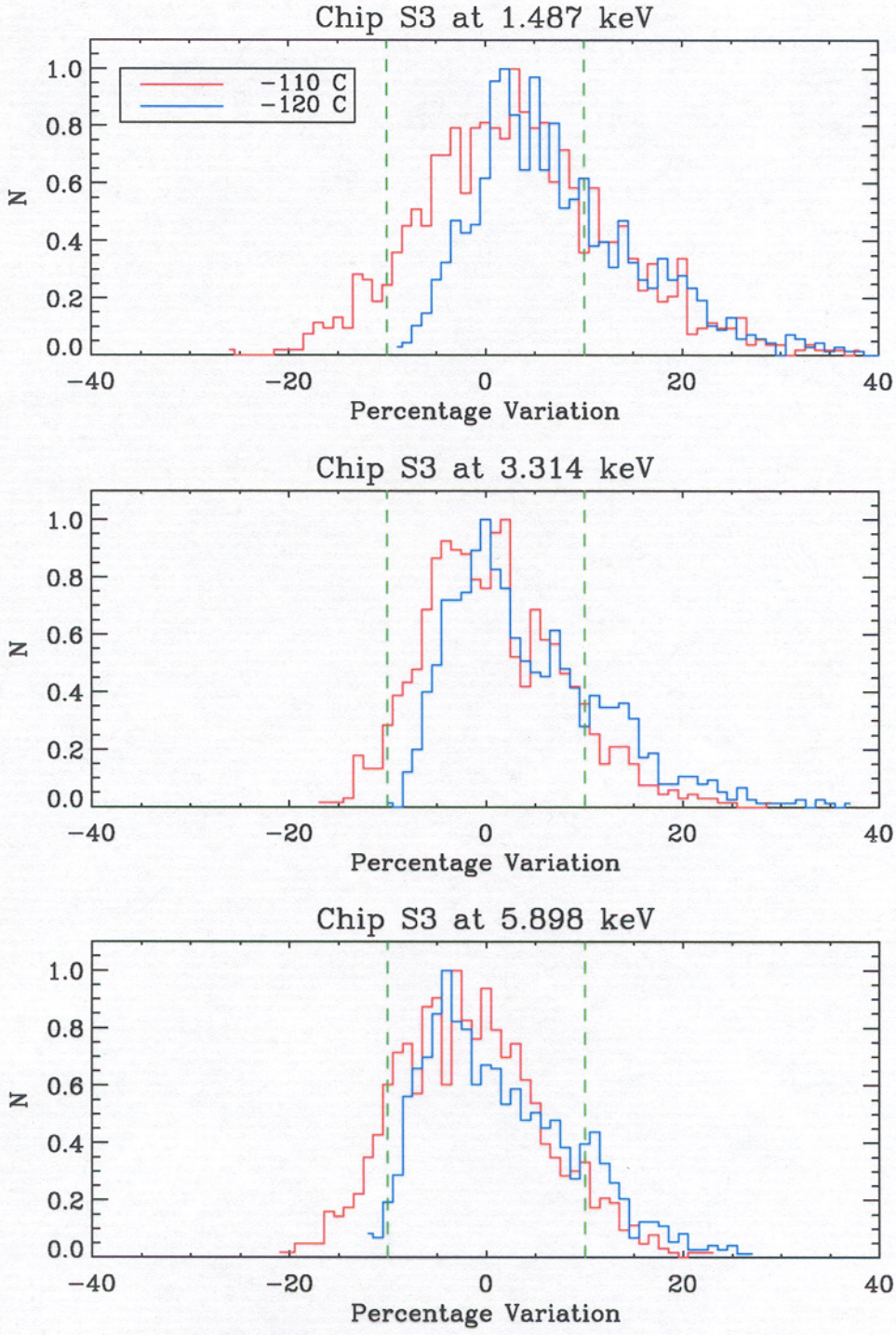

Figure 8: Histogram of ACIS S3 Resolution Variations.

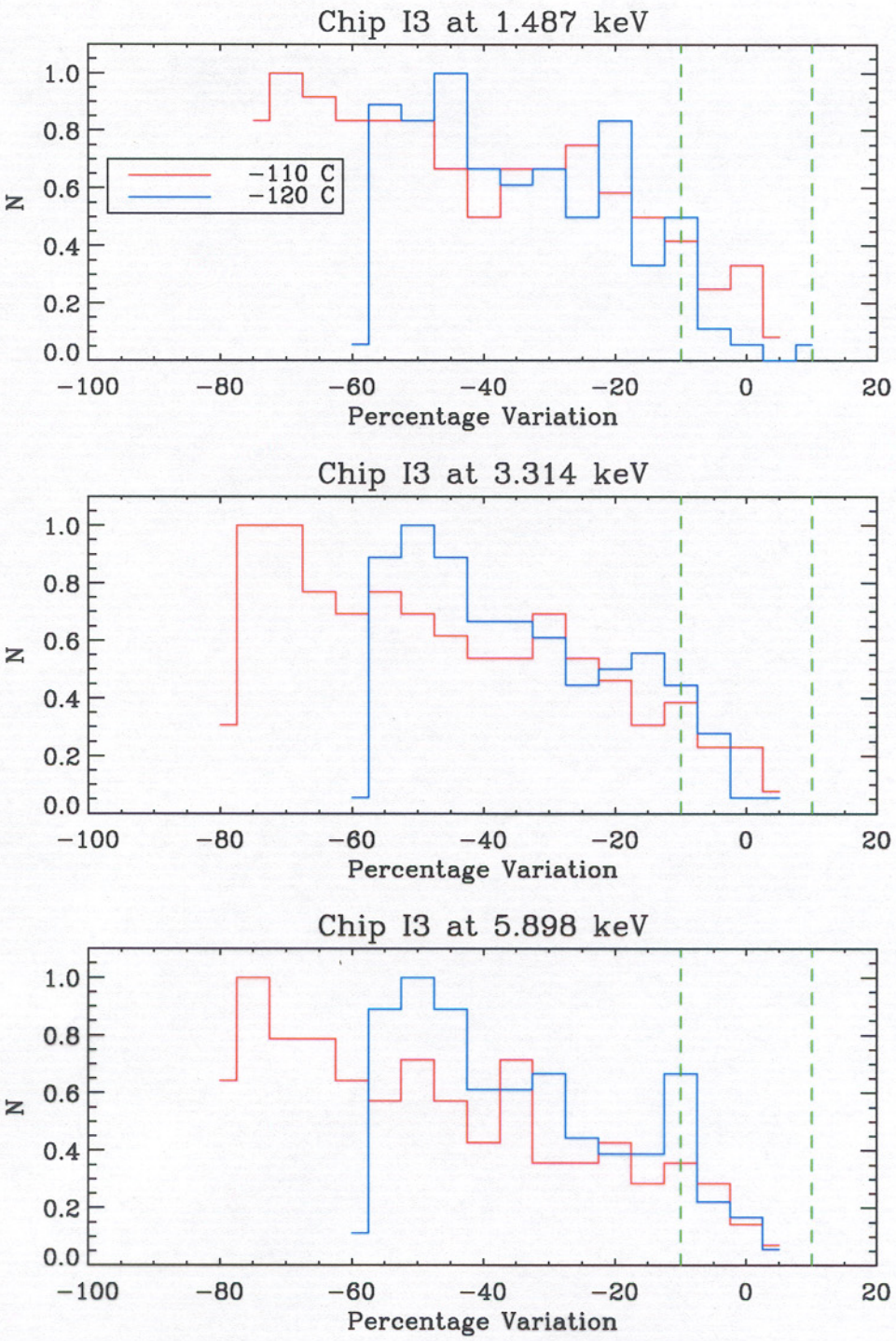

Figure 9: Histogram of ACIS I3 Resolution Variations.

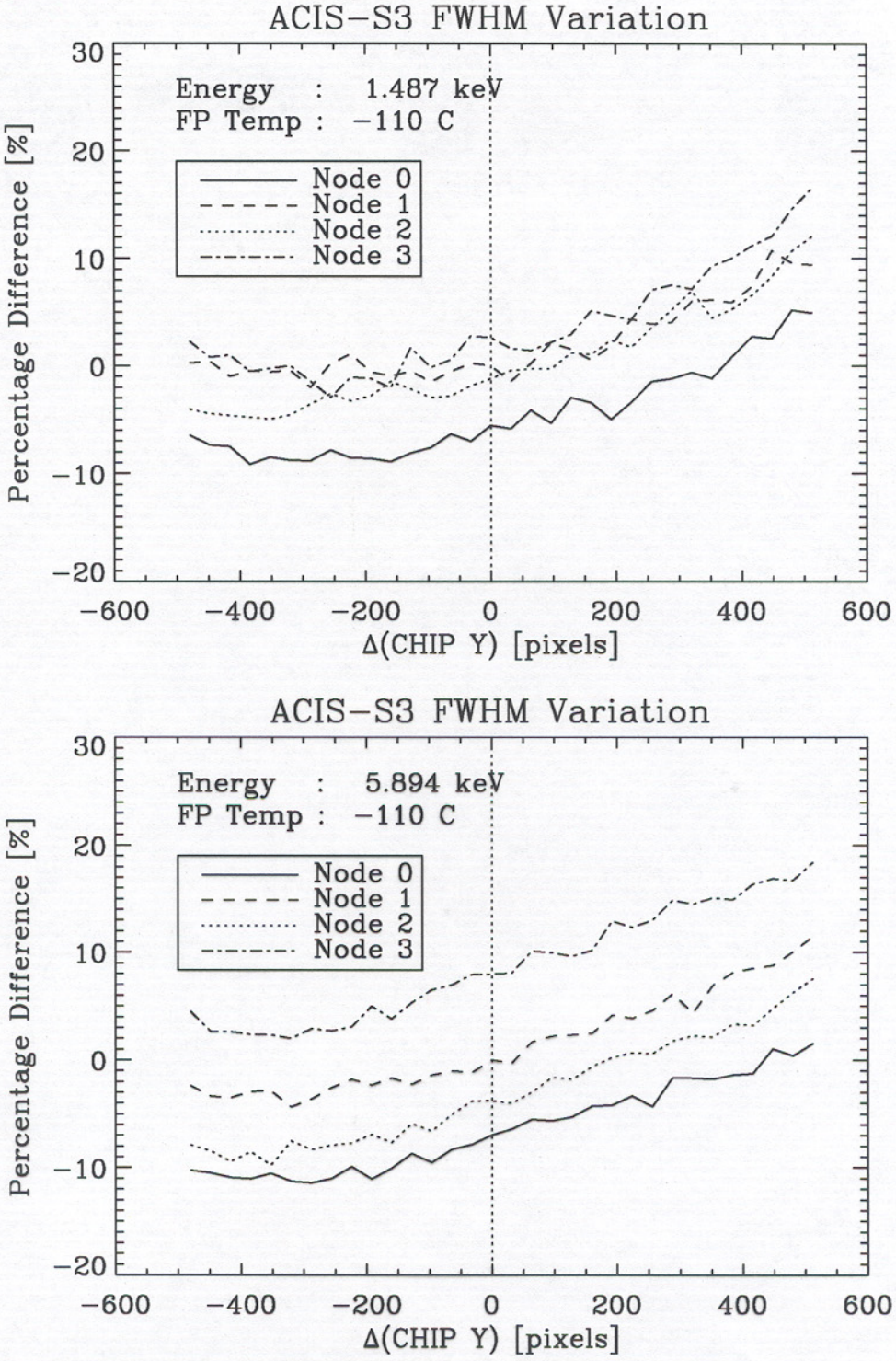

Figure 10: Variation in S3 FWHM Relative to the Aimpoint.

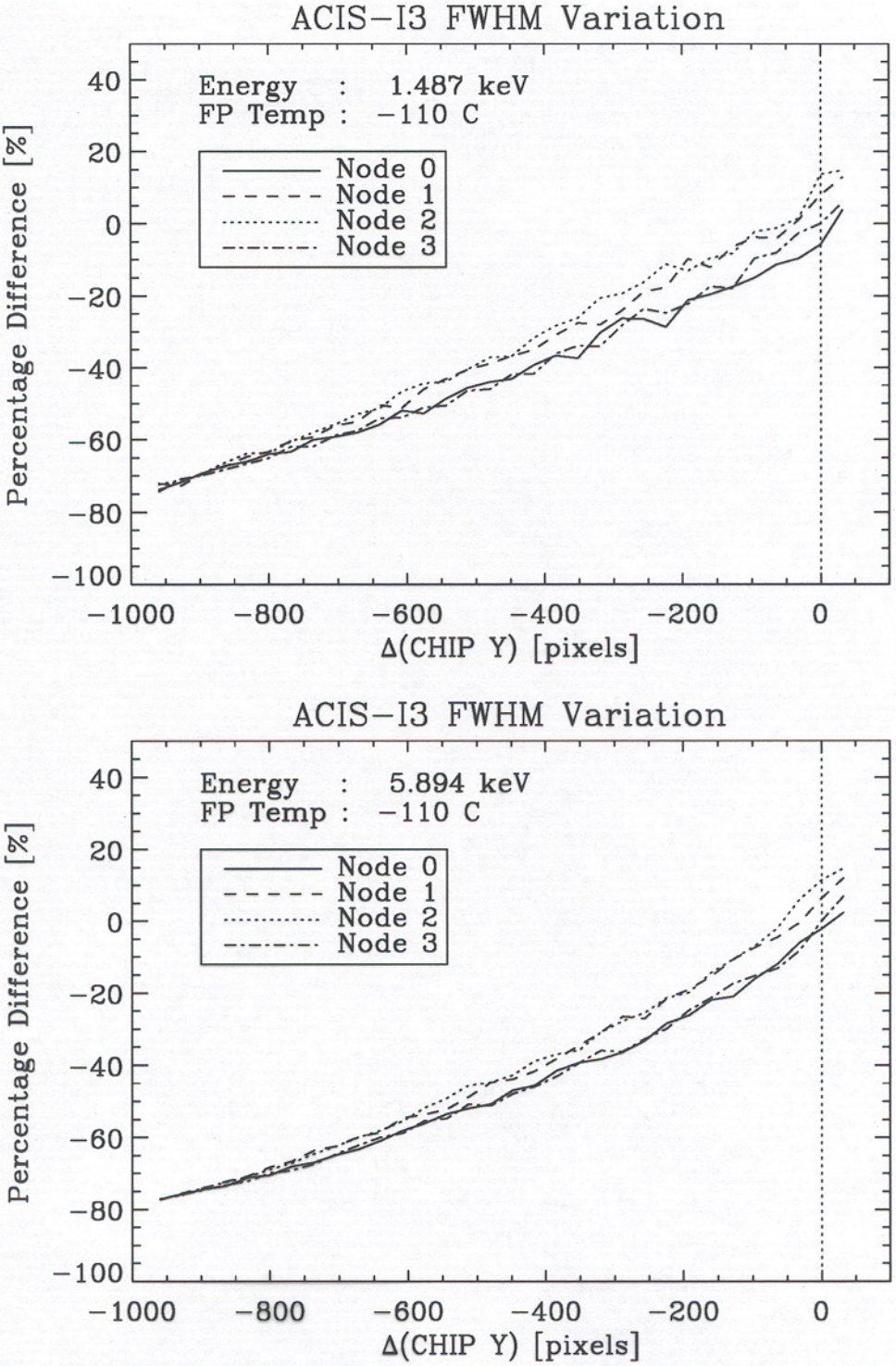

Figure 11: Variation in I3 FWHM Relative to the Aimpoint.

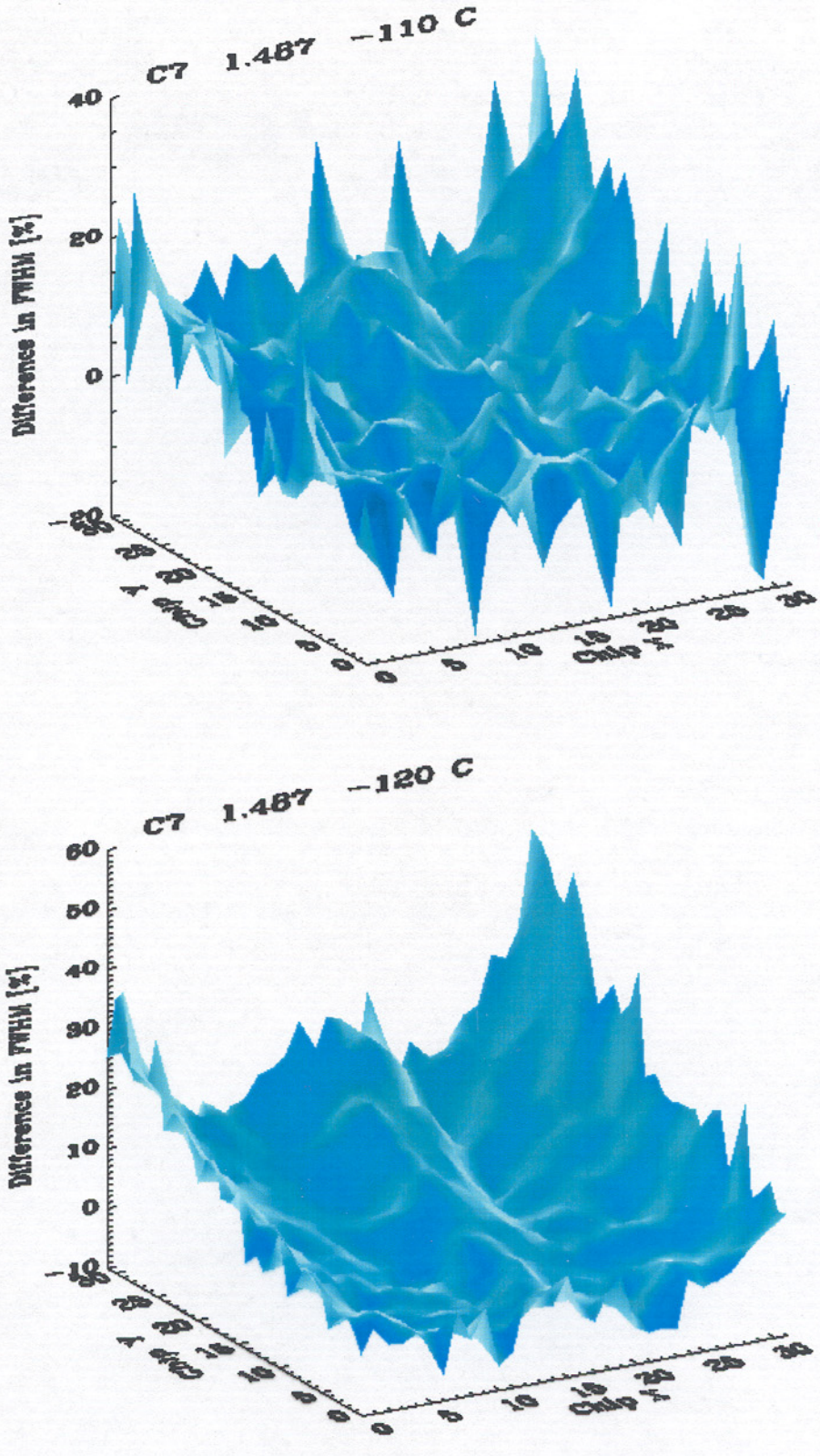

Figure 12: ACIS FWHM variations for S3 at 1.487 keV.

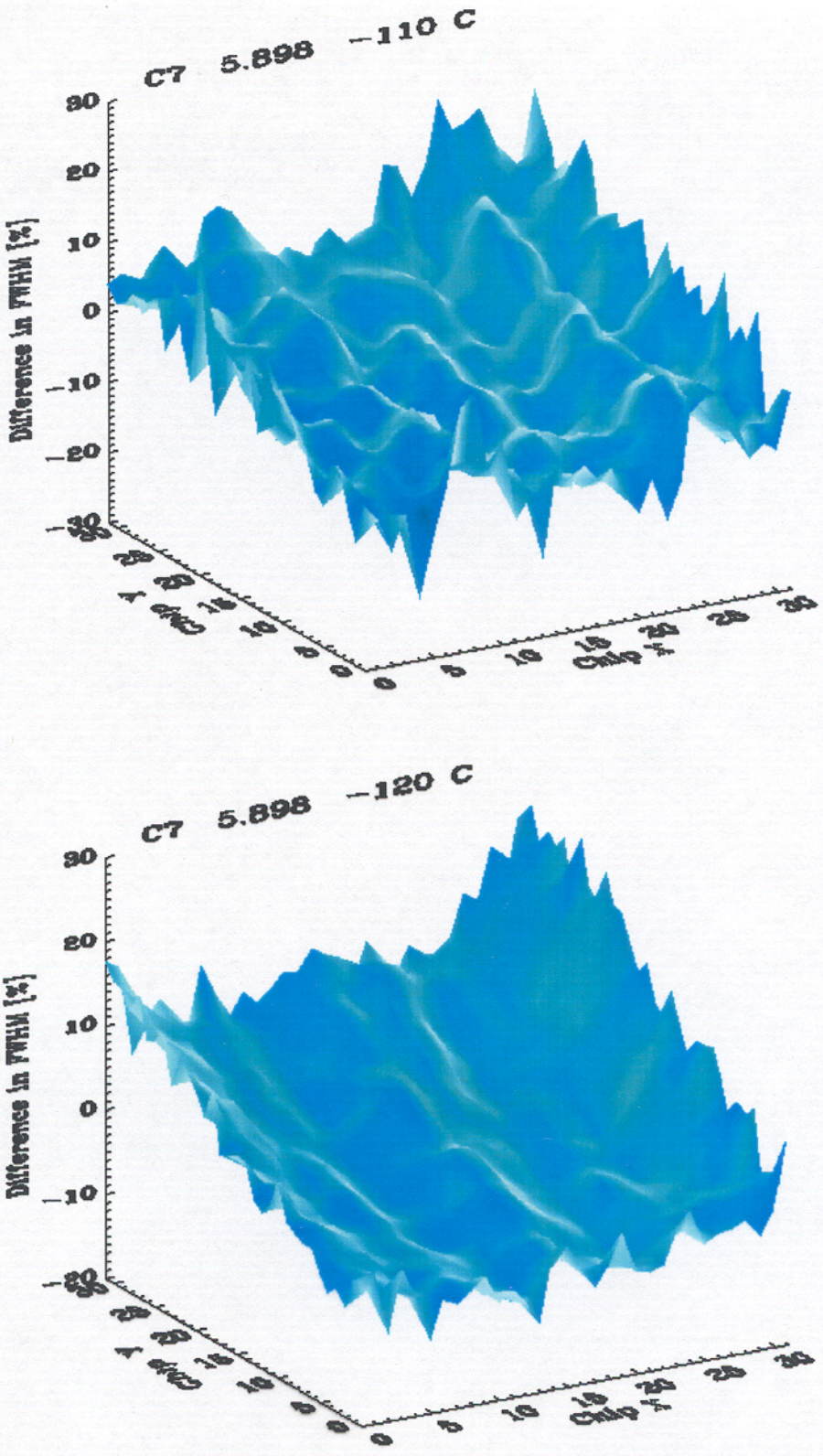

Figure 13: ACIS FWHM variations for S3 at 5.898 keV.

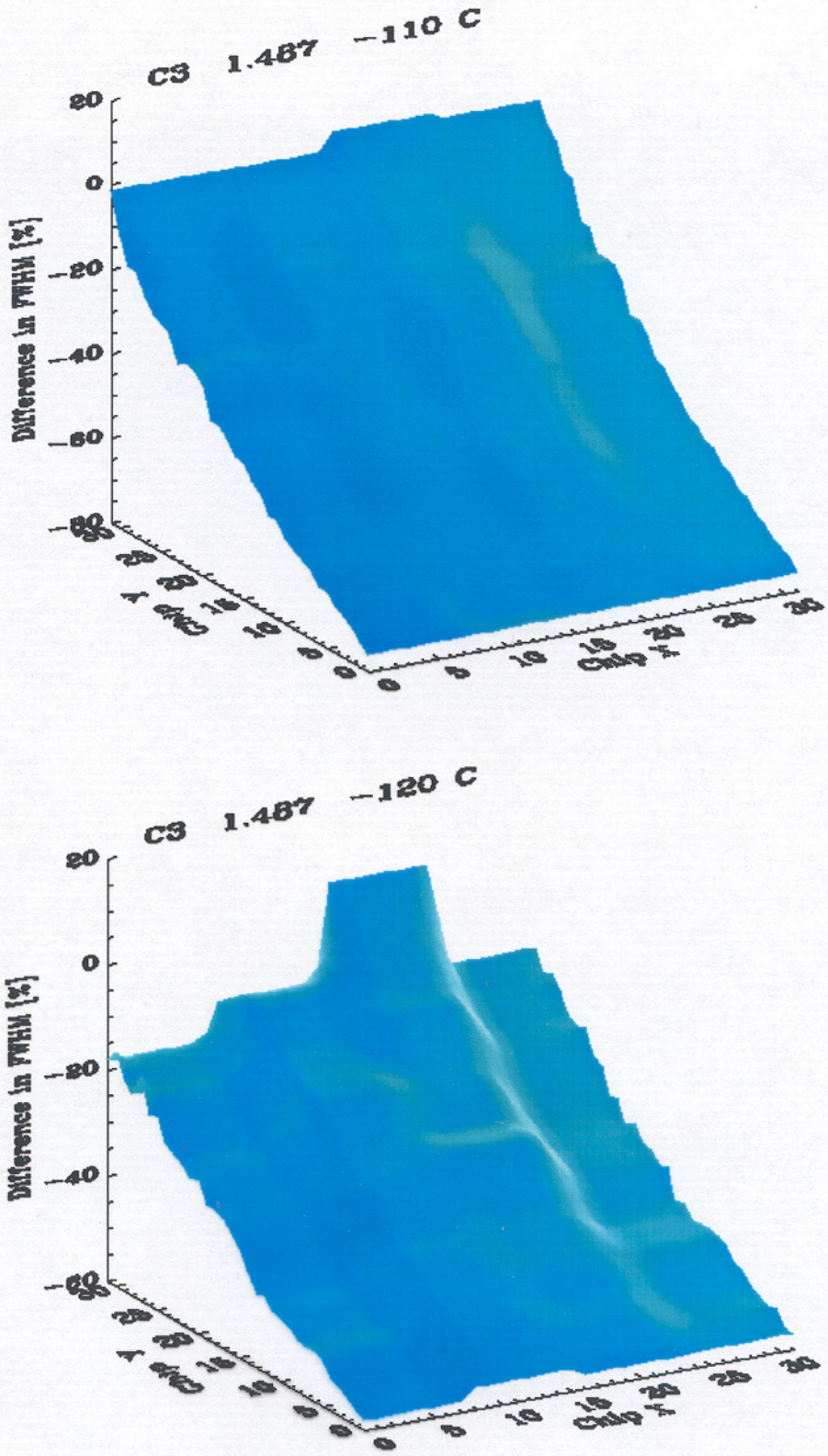

Figure 14: ACIS FWHM variations for I3 at 1.487 keV.

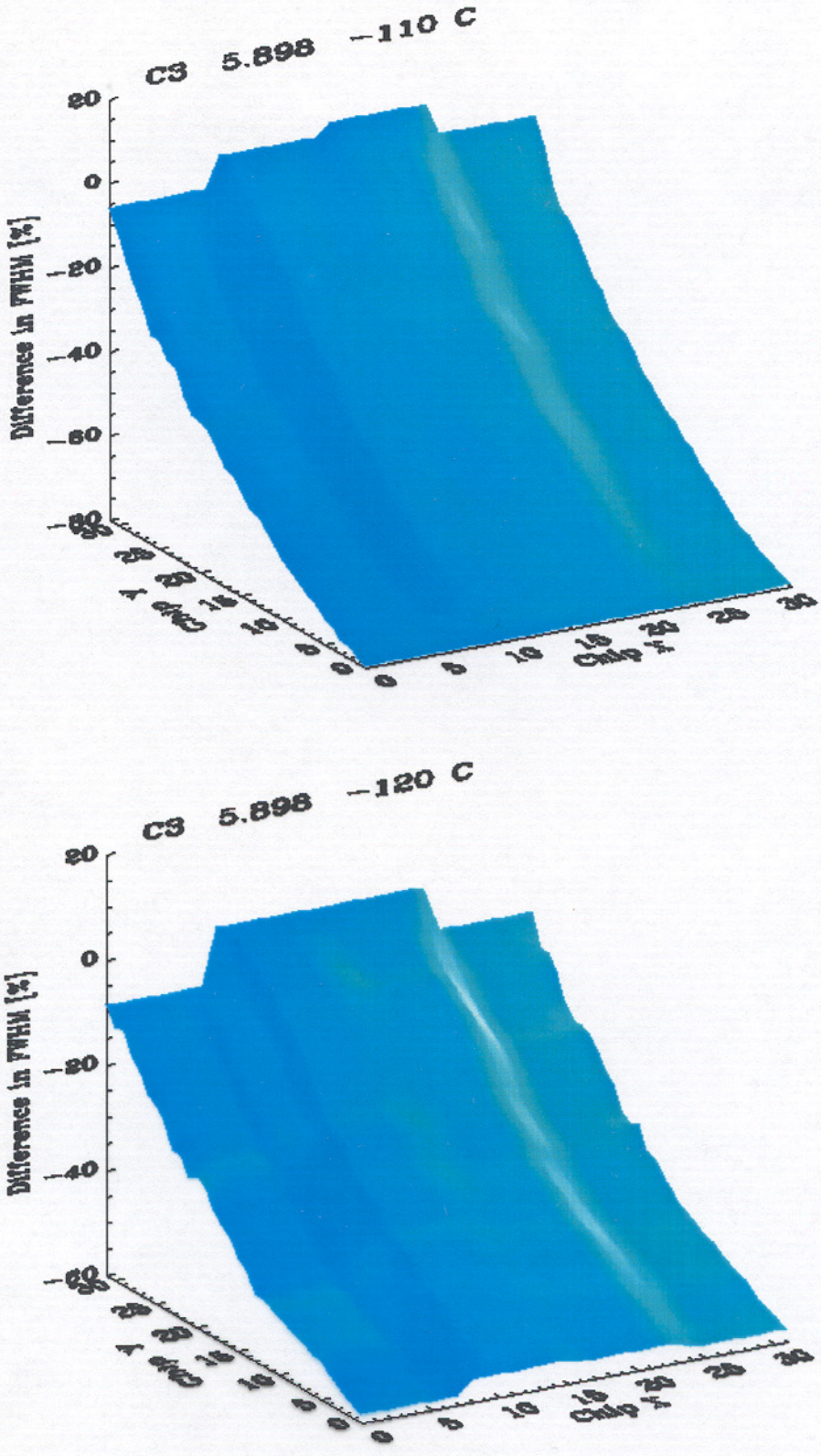

Figure 15: ACIS FWHM variations for I3 at 5.898 keV.

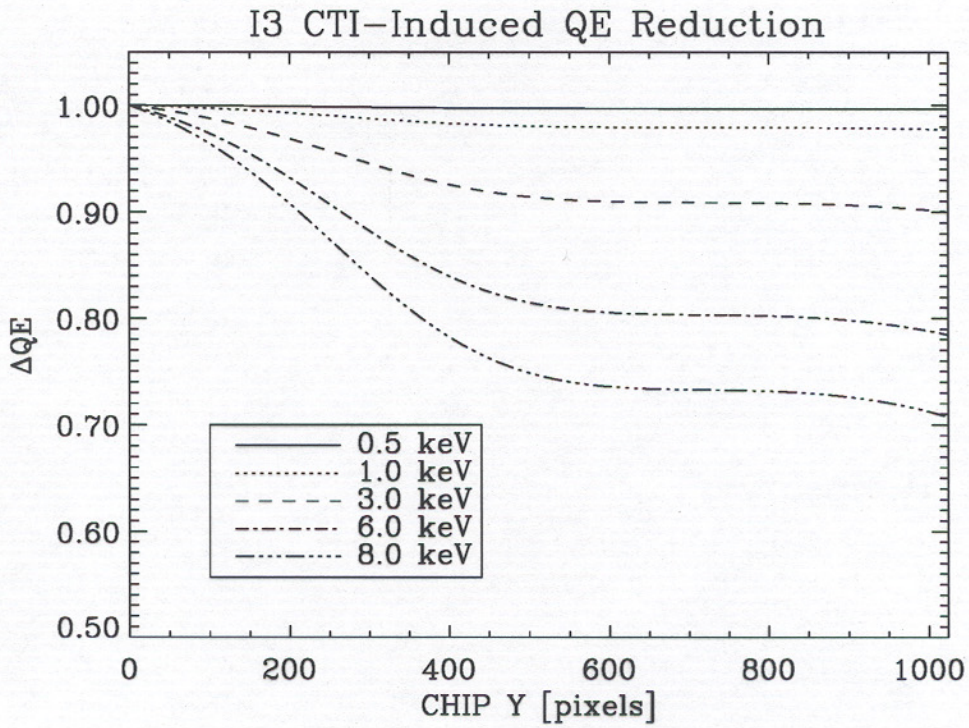

Figure 16: Variation in I3 quantum efficiency due to CTI.

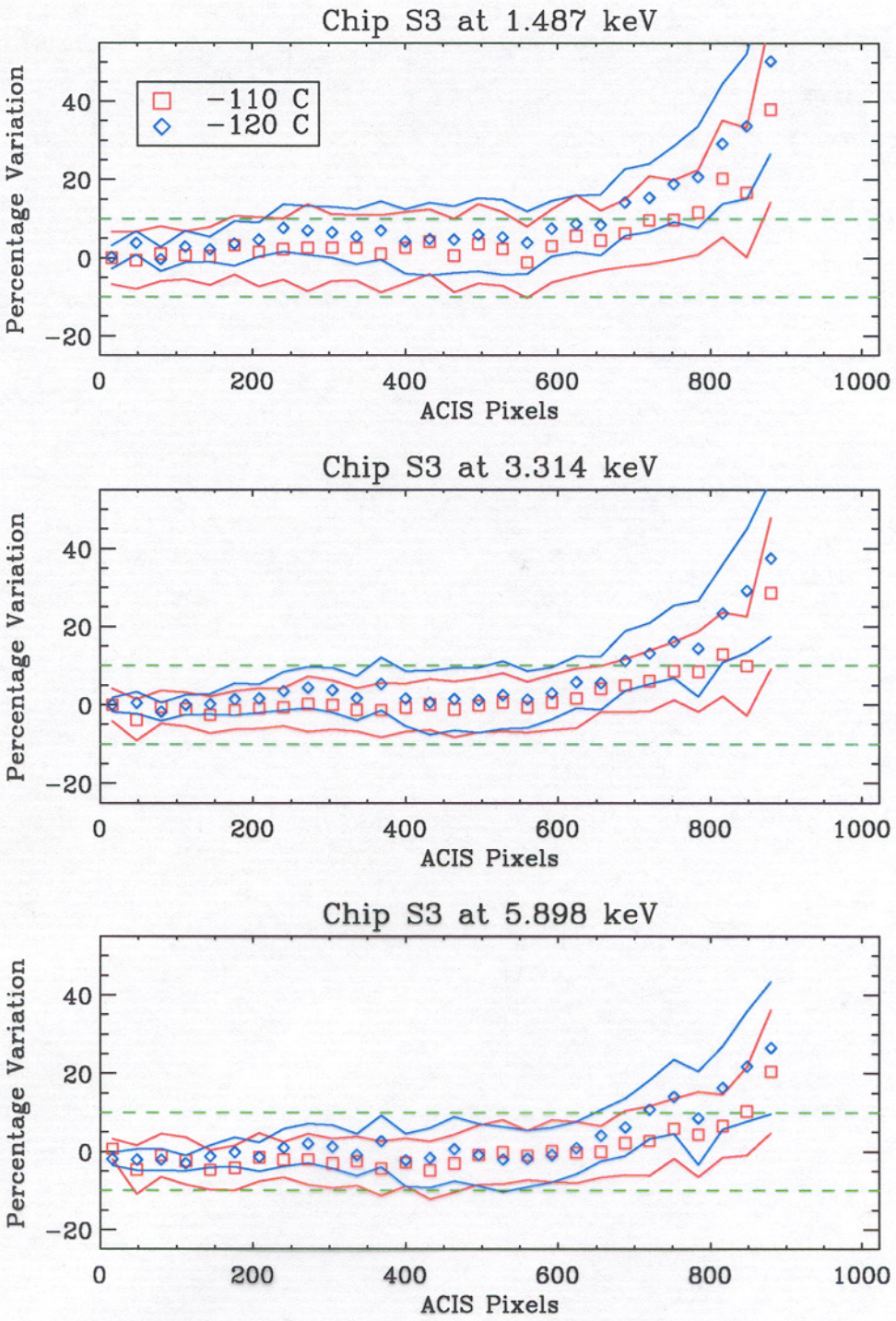

Figure 17: Radial Resolution Variation on ACIS S3 relative to aimpoint.

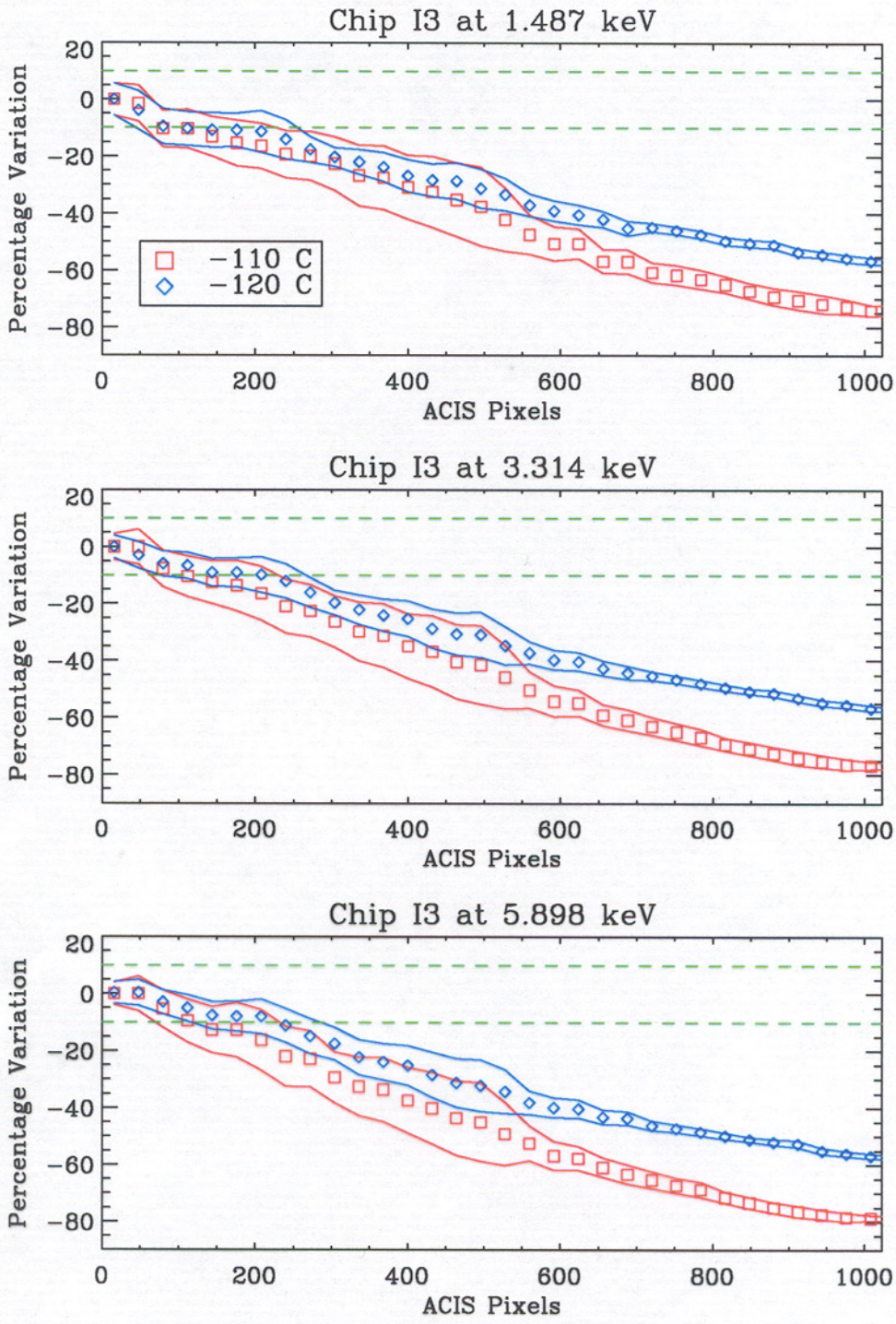

Figure 18: Radial Resolution Variation on ACIS I3 relative to aimpoint.

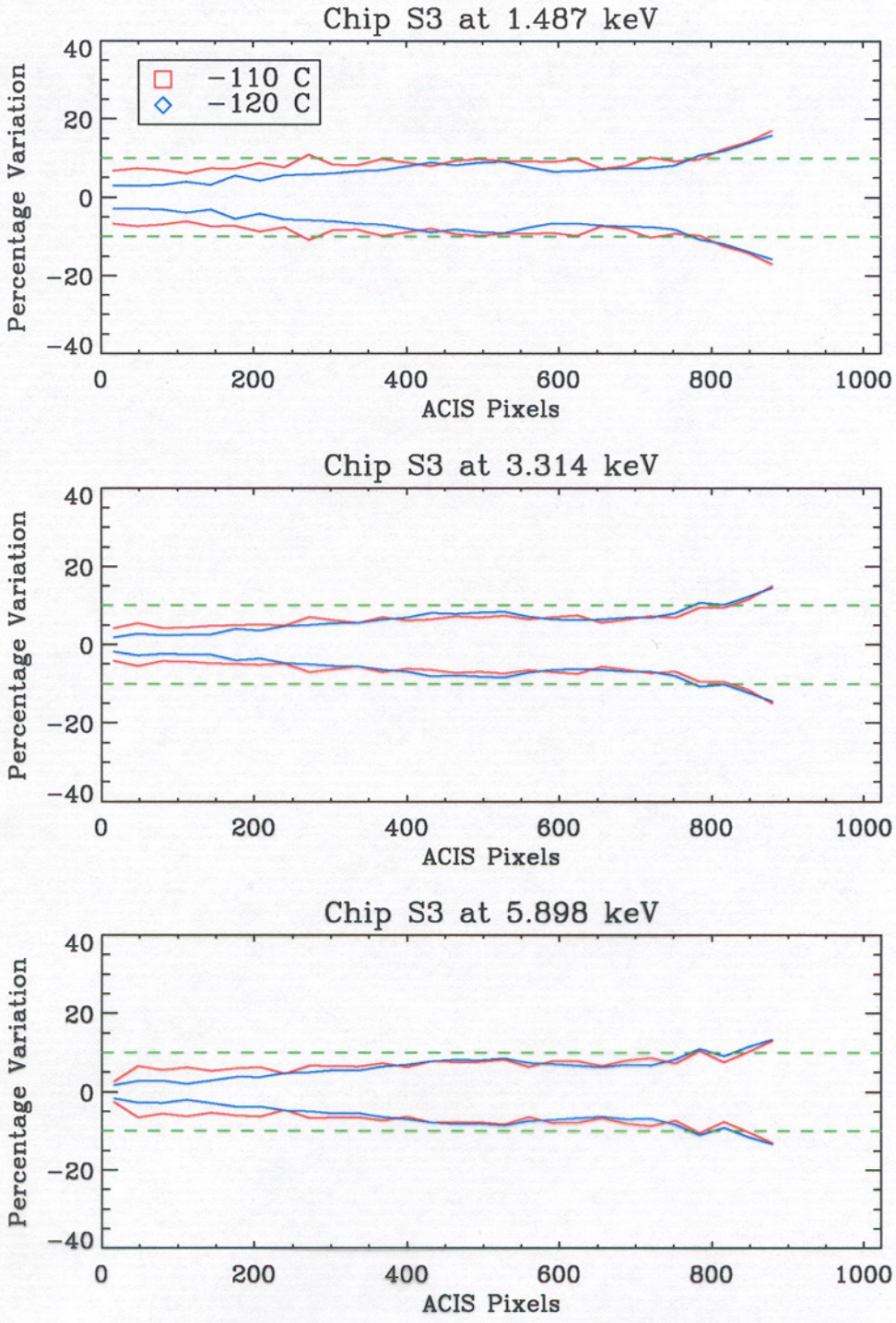

Figure 19: Local Radial Resolution Variation on ACIS S3.

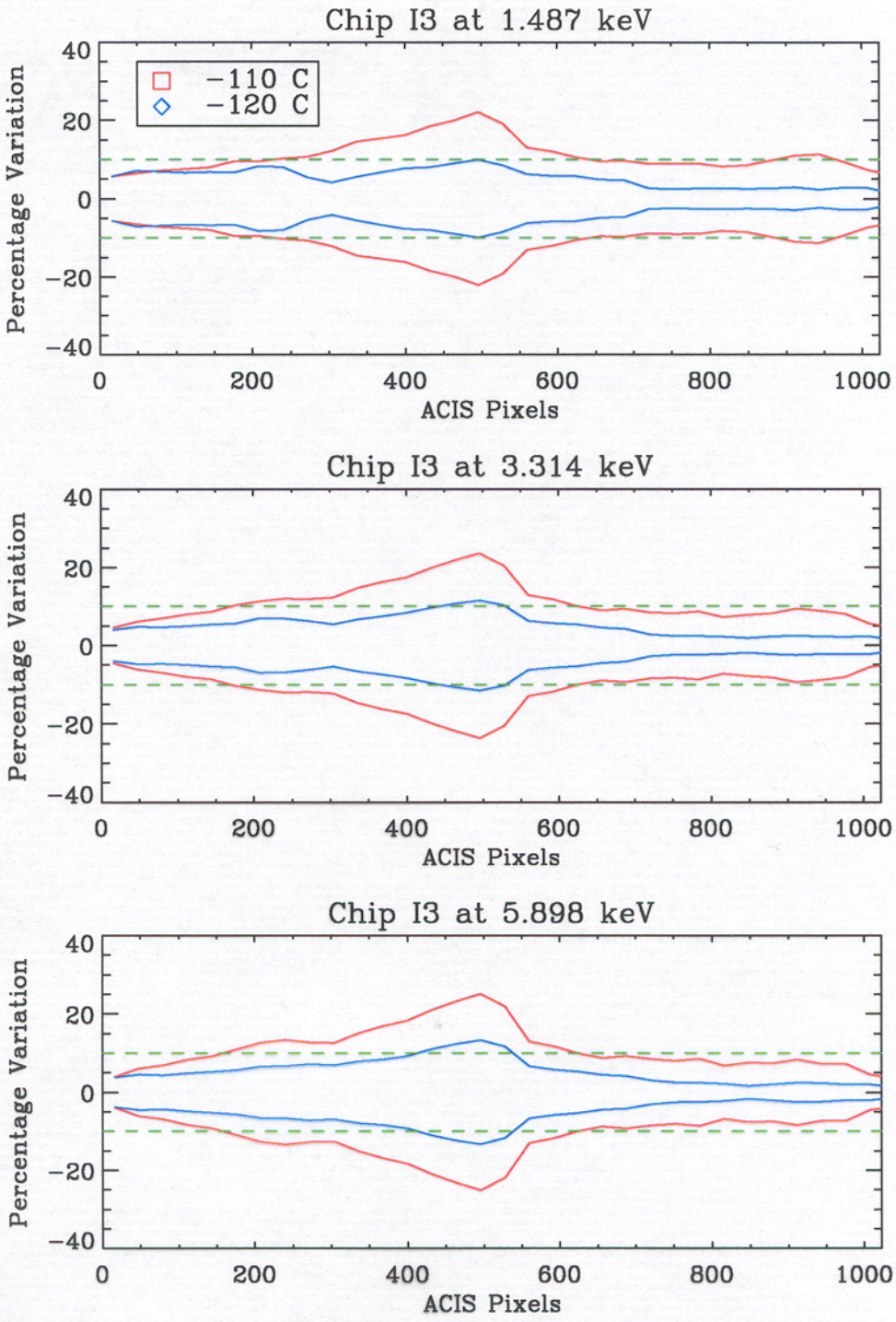

Figure 20: Local Radial Resolution Variation on ACIS I3.

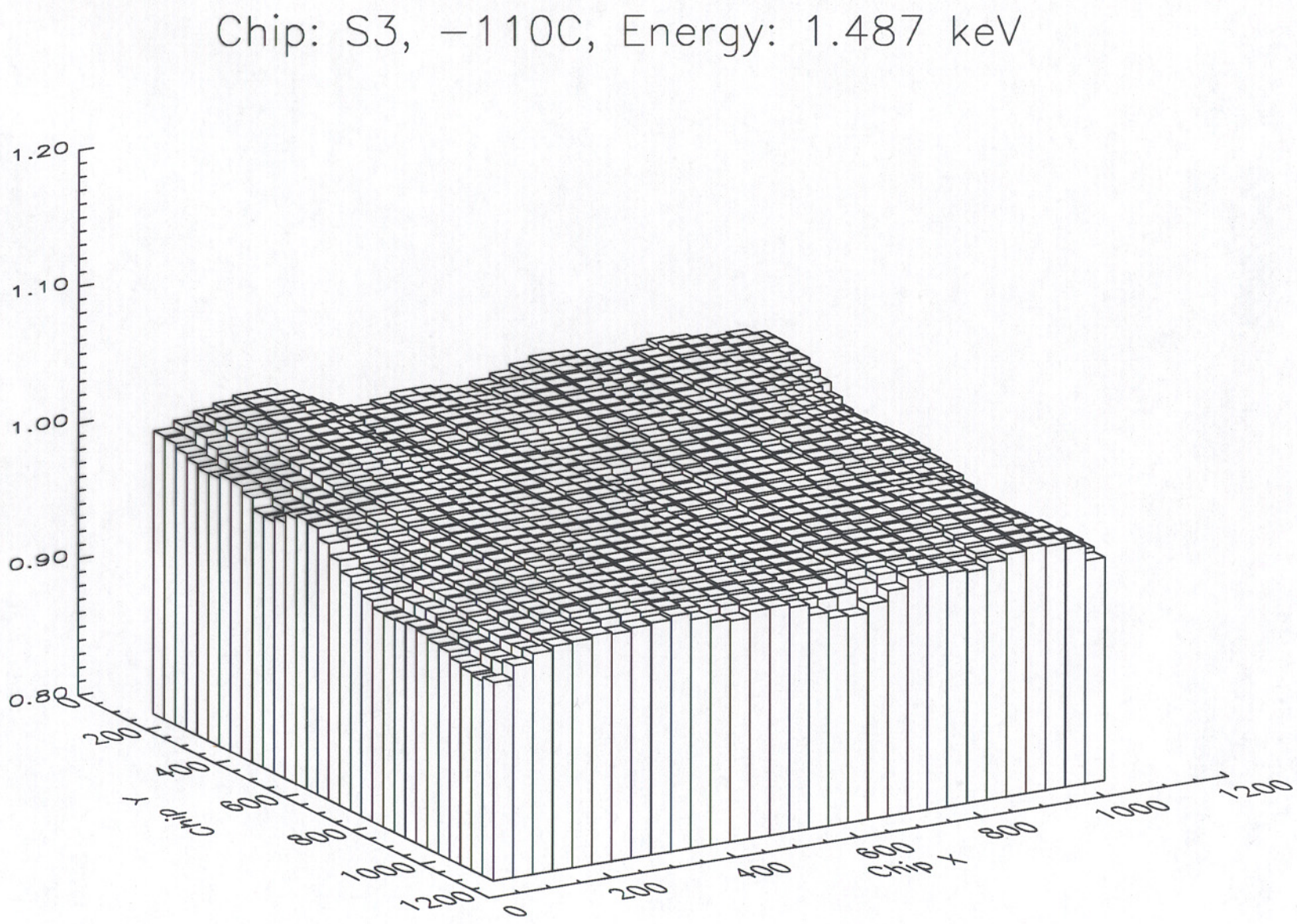
Chip: S3, −110C, Energy: 1.487 keV
1.20
1.10
1.00
0.90
0.80
200
400
600
800
1000
1200
Chip Y
0
200
400
600
800
1000
1200
Chip X
MIT/CXC Tue Jun 27 11:19:07 2000

Chip: S3, −120C, Energy: 1.487 keV

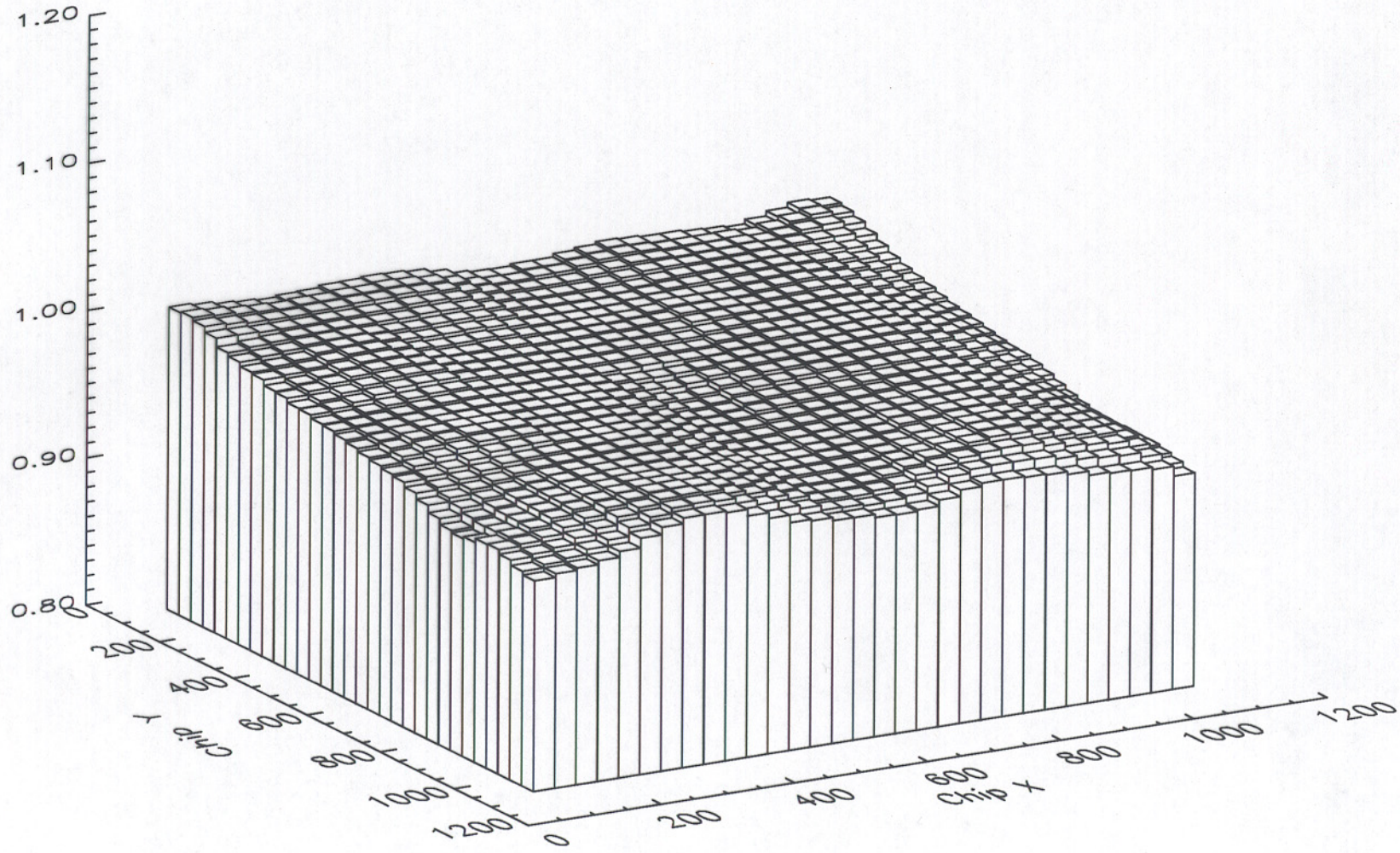

MIT/CXC Tue Jun 27 12:03:02 2000

Chip: S3, −110C, Energy: 5.898 keV

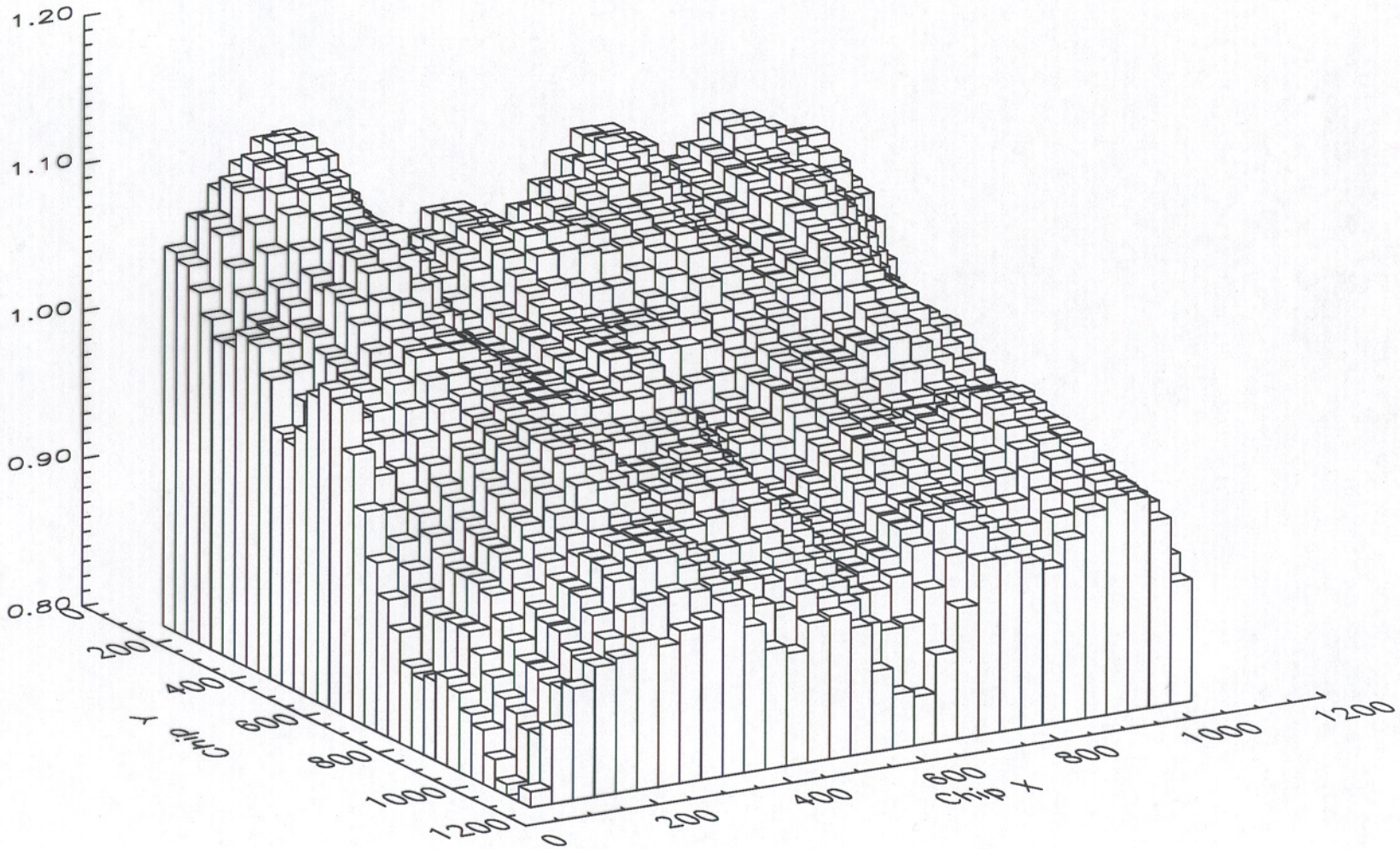

MIT/CXC Tue Jun 27 11:19:07 2000

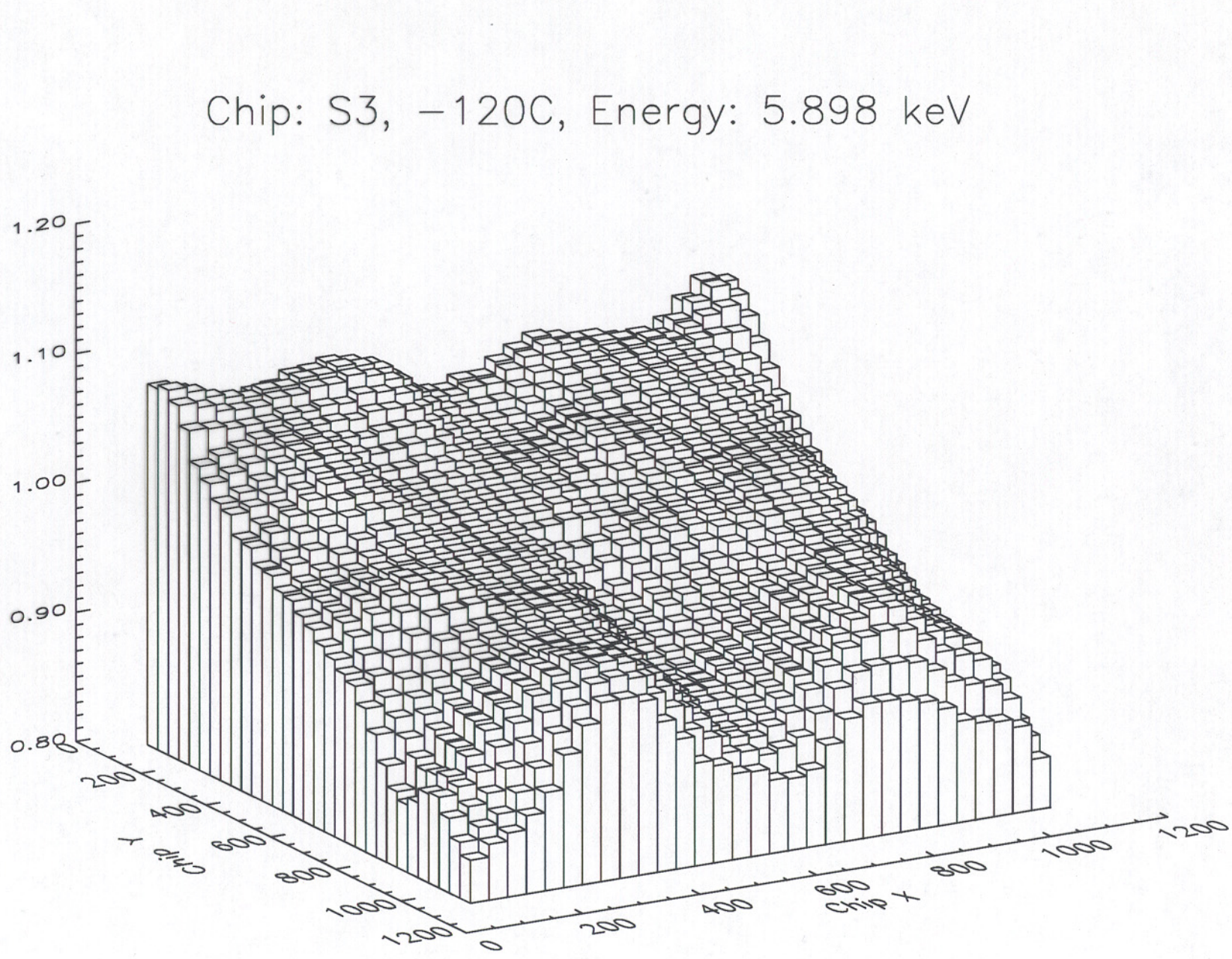
Chip: S3, −120C, Energy: 5.898 keV
1.20
1.10
1.00
0.90
0.80
200
400
600
800
1000
1200
Chip Y
0
200
400
600
800
1000
1200
Chip X
MIT/CXC Tue Jun 27 12:03:02 2000

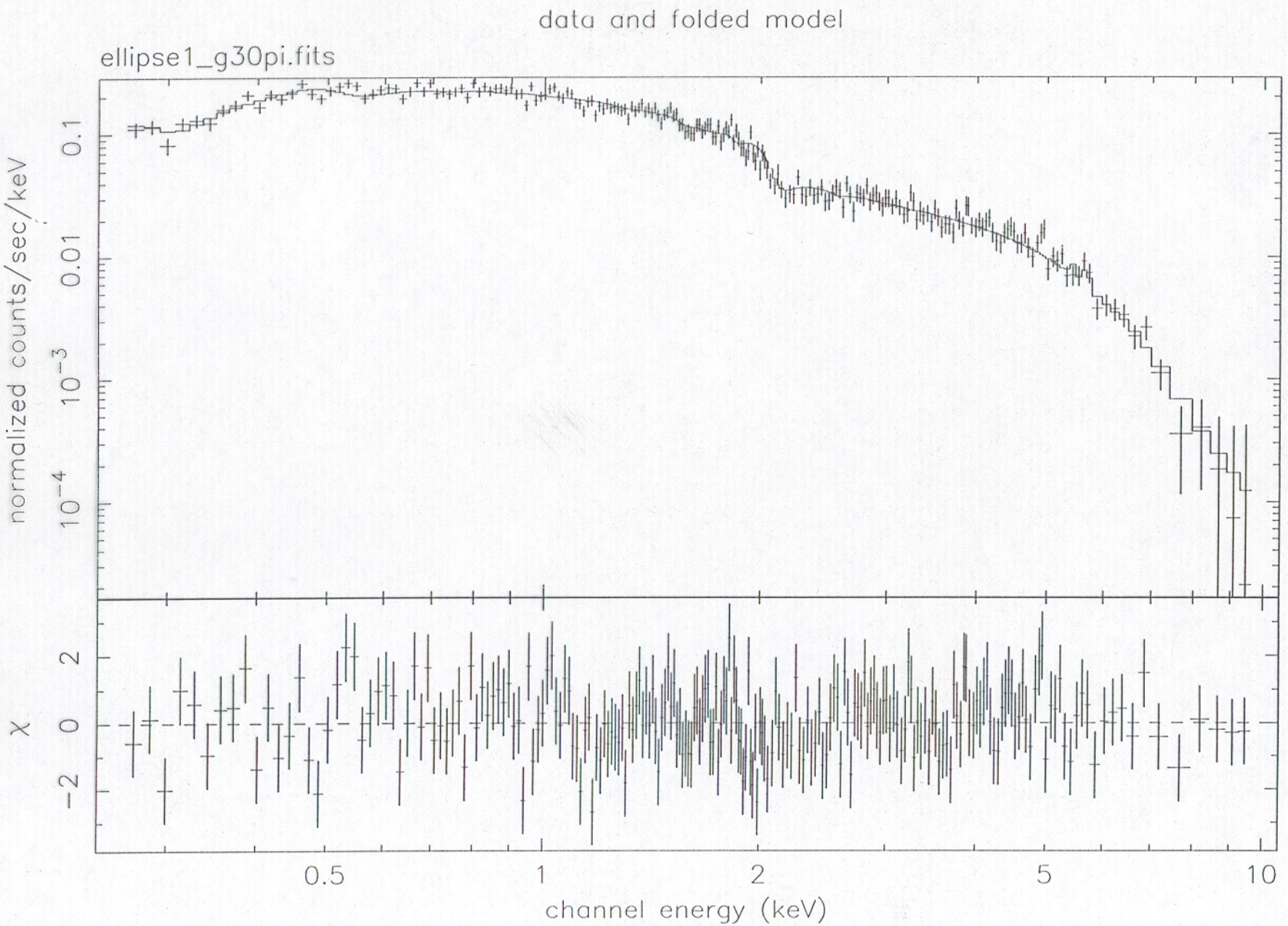

houck 21-Jun-2000 13:30

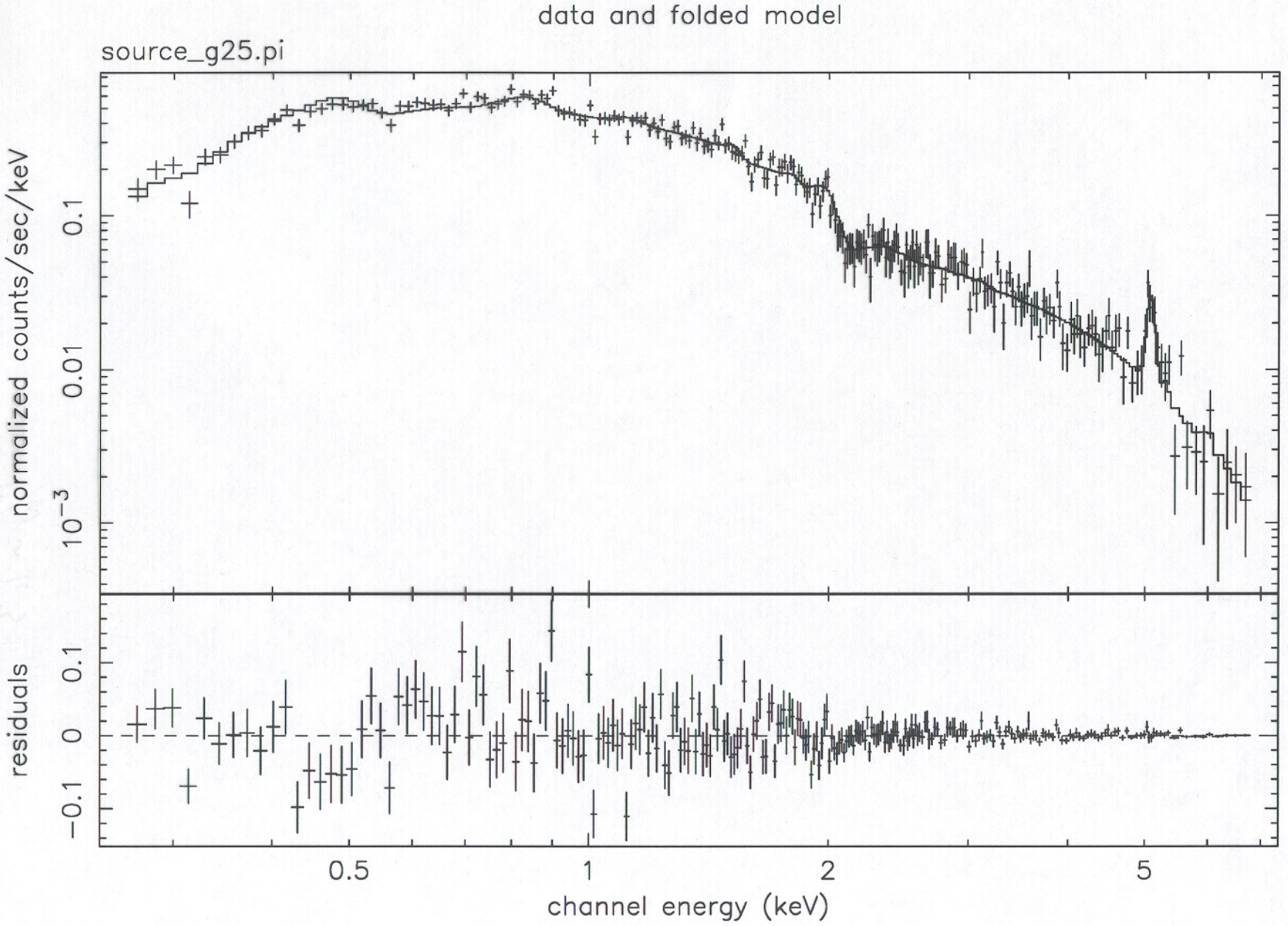

wise 29–Jun–2000 18:36